Muxworthy, AR, Schmidbauer, E, Petersen, N, **Magnetic properties and Mossbauer spectra of urban atmospheric particulate matter: a case study from Munich, Germany**, GEOPHYS J INT, 2002, Vol: 150, Pages: 558 - 570, ISSN: 0956-540X

Magnetic properties and Mössbauer spectra of urban atmospheric particulate matter: A case study from Munich, Germany.

A. R. Muxworthy∗, E. Schmidbauer and N. Petersen.

Institut für Allgemeine und Angewandte Geophysik, Universität München, Theresienstrasse 41, 80333, Munich, Germany.

14 May 2001, revised 13 February 2002

Summary

Due to the high concentrations of iron in anthropogenically-derived atmospheric particulate matter (PM), magnetic techniques are ideal for the study of the behaviour of PM. However, to undertake these studies it is necessary to have a thorough understanding of the magnetic mineralogy of PM. This study reports a detailed examination of the magnetic mineralogy of PM samples collected in Munich. Several different approaches have been utilised in the characterisation; from standard mineral magnetic techniques such as magnetic hysteresis and microscopy to non-standard techniques such as Mössbauer spectroscopy. In particular, the study has focused on the smallest magnetic grains (< 30 nm), which are mostly likely to be inhaled into the human lung. These have been characterised using low-temperature magnetic and Mössbauer measurements, in conjuncture with the standard frequency dependency of magnetic susceptibility measurements. The primary magnetic minerals were found to be maghemite and metallic iron. The mean magnetic grain size range for these two minerals was 0.1-0.7 μm. The magnetic signature was estimated to come from 60-70% maghemite and the rest from metallic iron. A significant percentage of maghemite in the grain-size range 10-16 nm was identified, and there was evidence for metallic iron in the grain-size range 5-8 nm. This latter fraction is of particular importance as transition metal particles < 10 nm in diameter are known to catalyse the production of free radicals which are known to cause many lung complaints such as asthma. It was difficult to give accurate estimates of the total magnetic content by mass due to the mixed mineralogy, however, the absolute limits for the total magnetic content was estimated to be between 0.02-1.2 %. It is suggested that the maghemite comes from automobiles and the metallic iron from the street-trams which run near the sampling site.

Key words: environmental magnetism, particulate matter**,** superparamagnetism.

1 Introduction

∗ Now at Dept. of Physics, University of Toronto, Toronto, Canada. email: adrian@physics.utoronto.ca

It is well known that atmospheric particulate matter (PM) can adversely effect human health, however, it is still unclear which physical and chemical properties of PM most strongly effect human health (Harrison & Yin, 2000). Epidemiological studies do not reveal whether it is the mass, size, number or surface area of the particles which is the most important determinant of health impact, though they do show that ultrafine particles (< 100 nm) exert a much greater physiological effect than the same mass of coarse particles (*e.g.,* Donaldson *et al.*, 1998). Hence, there is a need to understand both the nature and behaviour of urban PM and its grain-size distribution. Due to the high-concentrations of magnetic minerals in urban pollution PM, the strong relationship between the magnetic-signature of a mineral and its grain size particularly for grains less than 1 μm, and the rapid measurement time, the application of magnetic techniques to assess urban PM is being increasingly seen as a viable approach to study PM (*e.g.,* Matzka & Maher, 1999, Shu *et al.*, 2001).

Typical bulk iron content is found to constitute about 1 % of urban atmospheric PM (Department of the Environment, 1996), with iron oxides and hydroxides contributing 10-70 % of the bulk iron content (Dedik *et al.*, 1992; Weber *et al.*, *2*000). Much of this iron is associated with mobile sources, *e.g.*, vehicles. Iron impurities in fossil fuels convert on combustion to magnetic iron oxides, *i.e.*, magnetite, maghemite, hematite or a mixture, depending on the combustion conditions. Because of its combustion origin, magnetic PM is not only dangerous in itself due to iron's and iron oxides' catalytic nature (Phumala *et al.*, 1999; Garçon *et al.*, 2000), but it is also associated with other hazardous pollutants which are injected into the atmosphere during combustion (Morris *et al.*, 1995). PM in the vehicle exhaust is dominated by particles < 10 μm, *i.e.*, PM_{10} (Kim *et al.*, 2001). In addition to direct combustion derived particles, vehicles produce other magnetic PM from the mechanical wear of tires and brakes, and the ejection of particles from the pavement and unpaved shoulder by re-suspension processes (Olson & Skogerboe, 1975). The products of tire and brake wear and the re-suspended road dust are dominated by particles > 10 μm (Gillies *et al.*, 2001).

Previous magnetic studies have used the magnetic signature of PM to assess the behaviour of PM either through time (*e.g.*, Morris *et al.*, 1995; Muxworthy *et al.*, 2001), spatially (*e.g.*, Kapička *et al.*, 1999) or its association with heavy metals (*e.g.*, Hunt *et al.*, *1*984). However, if magnetic techniques are to be used to access PM behaviour, it is essential to have detailed characterisation of the magnetic minerals within urban PM. Previous characterisation studies have either measured the magnetic signature of particular PM types especially fly-ash (*e.g.,* Dekkers & Pietersen, 1992; Flanders, 1994; 1999) or have studied the magnetic properties of urban PM which is thought to be dominated by the signal from vehicles (*e.g.,* Xie *et al.*, 1999; Shu *et al.*, *2*001). Previous studies have shown that urban PM which is thought to be primarily vehicularly derived, consists of a dominant magnetite-like phase (Fe_3O_4) in the grain size range 0.3 μm to 3 μm in diameter (Matzka & Maher, 1999).

In addition to magnetic studies, there have been a number of studies which have used

Mössbauer spectroscopy to characterise the iron content within urban PM (*e.g.*, Mahieu *et al.*, 1976; Dedik *et al.*, 1992; Hoffmann *et al.*, 1996; Veranth *et al.*, 2000; Weber *et al.*, 2000; Kopcewicz & Kopcewicz, 1992; 1998; 2001). These studies found site-specific results; Mahieu *et al.* (1976) detected maghemite/hematite, Fe^{2+} ions and Fe^{3+} ions in their urban PM samples, and Kopcewicz & Kopcewicz (1992; 1998; 2001) have found high levels of iron sulphides related to coal usage as a local form of house heating, in addition to iron hydroxides and iron oxides in their studies in Poland. High concentrations of goethite were found in air-conditioning PM from Darmstadt, with lower concentrations of magnetite, hematite, Fe^{2+} ions and Fe^{3+} ions (Dedik *et al.*, 1992; Hoffmann *et al.*, 1996; Weber *et al.*, 2000). However, with respect to the Darmstadt studies it is suggested in Weber *et al.* (2000), in an attempt to explain the discrepancy between Mössbauer spectroscopy and transmission electron microscopy (TEM) observations, that the detection of goethite using Mössbauer spectroscopy was due to surface layers of water on nanometre-sized hematite (10 nm) particles.

In this paper we combine Mössbauer spectroscopy and magnetic results in a detailed characterisation of urban atmospheric PM collected in Munich in 1999 and 2000. PM collectors was designed and constructed. The samples were also examined using scanning electron microscopy (SEM).

2 Sampling and Methodology

The nature of the collection method strongly influences both the physical and chemical nature of a sample. In the literature several different techniques have been employed to collect PM samples for magnetic study; firstly filter methods (*e.g.,* Morris *et al.*, *1*995; Shu *et al.*, *2*001), secondly collecting street dust (Xie *et al.*, 1999; 2000), and lastly by “biomonitoring”, *i.e.*, sampling leaves with deposited PM (Matzka & Maher, 1999). All three methods have problems in that none of them sample the total PM grain-size distribution. With the filter method it is suggested the very smallest particles will pass straight through the filter and will not be collected. However, the degree to which this is a problem is uncertain as the smallest particles (< 10 nm in diameter) usually agglomerate within the first 10 minutes (Department of the Environment, 1996). The street dust method of collection, *i.e.*, dust collected directly from the street or pavement, suffers in that the material collected tends to be on average considerably larger than the mean PM residing in the air, and is consequentially not representative of PM which is inhaled. For example, the frequency dependency of magnetic susceptibility (χ_{FD}) which is related to the smaller grain size fraction, is considerably higher for samples collected by filter methods than from street dust samples (*cf.*, Xie *et al.* (1999) and Shu *et al.* (2001)). The third method, biomonitoring, has many advantages over the other methods, but there are still problems in determining the amount of dust collected on the leaves, extracting the magnetic minerals from the leaves for, *e.g.*, thermomagnetic analysis, consistency between tree species and it is uncertain if the PM collected is truly representative of the airborne PM. The Mössbauer spectroscopy studies of PM have also used a range of collection methods; air-conditioning filter systems (Dedik *et al.*, 1992; Hoffmann *et al.*, 1996; Weber *et al.*, 2000), filters (Mahieu *et al.*, 1976; Kopcewicz & Kopcewicz, 2001) or electrostatic precipitators (Mahieu *et*

al., 1976).

In an attempt to resolve the problems of collecting a representative PM sample two versions of PM collectors were constructed. The first type of PM collector consisted of circular frame covered in plastic sheets. The diameter of the frames were either 2 m or 1.4 m. At the centre of the plastic sheet a small hole was made. Initially the sheets were carefully cleaned with isopropanol, then the PM collector was left for the allotted time and the fallout collected. To collect the PM the plastic sheets were carefully cleaned with isoproponal and the mixture of suspended PM in alcohol drained through the small hole into a container. In addition, this first model had a manual roof which was used during rain to prevent the loss of the previously collected PM. The second model was similar; it consisted of a 1 m^2 plastic tray, with an automatic roof sensitive to rain. The use of the plastic tray allowed for the application of a thin layer of Klever GmbH Ballistol oil. The Ballistol oil was applied at the beginning of the collection period, and it did not evaporate during the collection period. The oil was applied because it was thought that PM collected on a dry surface had a high chance of being removed by the wind during the collecting period. This effect was thought to apply especially to the smallest particles. The oil and PM were collected in a similar method as described for the first version of PM collector.

For both models PM fallout was collected over sampling periods of three to four weeks duration. The first models were built in the summer of 1999 and placed at two locations near the Institute of Geophysics in the autumn of 1999. Location 1 was approximately 15 m from Barerstrasse and location 2 approximately 80 m from the same street. Barerstrasse is situated near the centre of Munich, and as well as vehicle traffic it also has electric street-trams. Samples were collected in the second model in the autumn of 2000. The details of the eleven samples collected are summarised in Table 1.

After collection the PM/isopropanol solution was wet-sieved with isoproponal through a 250 μm sieve to remove large objects such as leaves which had fallen into the collector. The isoproponal was then allowed to evaporate. For the samples collected without oil, the remaining PM was in a relatively fine powder form. For the samples collected using oil after evaporation of the isopropanol the PM/oil samples were mixed with Merck paraffin (no. 7337, melting point = 56-58 °C) at a temperature just above the melting point. On cooling to room temperature the oil and the paraffin coalesced to produce a solid matrix with the PM fixed with in it. The samples were then suitable for making Mössbauer and magnetic measurements.

^{57}Fe Mössbauer spectra were measured with a conventional spectrometer using a constant acceleration drive and an 512-multichannel analyser (γ-radiation source ~ 12mCi of ^{57}Co/Rh). The spectrometer was calibrated with sodium nitroprusside and metallic iron. All isomer shift data are given with reference to metallic iron. A liquid N_2 cryostat was available which allowed spectra to be recorded down to ~ 85 K, which helps to assess the presence of the smallest particles. The samples were pressed inside a standard Mössbauer holder (area ~ 2 cm^2). All sample densities were below ~ 5 $mgcm^{-2}$ of natural Fe. Depending on the source Co strength,

the measuring time took up to two weeks to measure one spectrum. The spectra were analysed by means of a least-squares fitting procedure using Lorentzian line shapes.

A suite of rock magnetic measurements were conducted on the samples. These measurements included hysteresis and thermomagnetic measurements at a range of temperatures between 80 K to 600 °C measured on two variable field translation balances (VFTB). The hysteresis measurements were originally made on a more sensitive VFTB ($\approx 1\times10^{-8}$ Am^2) which has a maximum field of 230 mT. Latterly, the hysteresis loops of some samples were re-measured using a second VFTB which has a larger maximum field (950 mT) and a liquid N_2 cryostat, but is less sensitive ($\approx 3\times10^{-8}$ Am^2). Typical sample weights were 50-100 mg. As with the Mössbauer spectroscopy, measuring at both room temperature and lower temperatures provides information about the smallest grains. Not all the samples were re-measured on this second VFTB due to either lack of material or lack of sensitivity. High-temperature thermomagnetic curves were measured, and low-temperature thermomagnetic curves were measured for a few samples on the second VFTB. High-temperature susceptibility measurements were made on an Agico CS3 susceptometer to help determine mineralogy. All the heating experiments were conducted in air. The samples collected in oil and mixed with paraffin, could only be used in the room temperature and low-temperature measurements. The frequency dependency of magnetic susceptibility (χ_{FD}) was measured using a Bartington dual-frequency susceptibility probe (470 Hz and 4700 Hz), to help assess the smaller grain-size content.

In conjunction rotational hysteresis measurements were made using an in-house rotational hysteresis magnetometer with a maximum field of 1.6 T. Rotational hysteresis loss measurements give information about the influence of various kinds of anisotropies on irreversible magnetisation processes. In most conventional magnetic measurements both reversible and irreversible magnetisation processes contribute to the total magnetic signal, however, because in rotational hysteresis loss measurements only the irreversible magnetisation processes contribute, it is possible to examine small irreversible features which cannot normally be observed. In particular it is possible to identify an exchange anisotropy between a ferri- or ferromagnetic phase with a antiferromagnetic phase, *e.g.,* between a grain's magnetite core and a surface oxidation layer of hematite (Meiklejohn & Bean, 1957). Rotational hysteresis loss, W_{RH}, is the energy required to rotate a ferro- or ferrimagnet quasi-statically through 360° in a constant magnetic field (Bozorth, 1951; Stacey & Banerjee, 1974). W_{RH} is determined by measuring the torque, **T**, exerted on a sample during rotation, firstly clockwise then anti-clockwise or *vice versa*. W_{RH} is defined as one-half of the area enclosed by the **T** versus rotation angle α curves (Bozorth, 1951),

$$W_{RH} = \tfrac{1}{2} \int \mathbf{T}(\alpha)d\alpha = \tfrac{1}{2} \int \mu_o I_{\perp} d\alpha \qquad (1)$$

where $I_{\perp}$ is the magnetisation perpendicular to the instant rotation field H and μ_o is the permeability of free space. All other components of magnetisation I do not contribute and give $\mathbf{T}(\alpha)=0$. When the applied field is small the magnetisation makes only small reversible excursions about its original direction during field rotation. During full rotation, both the forward and reverse curves are reversible making $W_{RH} = 0$. Reversible curves are also obtained for high fields where the magnetisation vector is always parallel to the applied field. For intermediate values irreversible magnetisation processes become significant giving non-zero values for W_{RH}. Detailed theoretical interpretation of rotational hysteresis curves has been made for SD particles with uniaxial anisotropy of the Stoner-Wohlfarth (SW) type (*e.g.,* Jacobs & Luborsky, 1957). Current knowledge of MD behaviour is more qualitative (*e.g.*, Keller & Schmidbauer, 1999; Muxworthy, 2002).

For the rotational hysteresis, the PM samples were carefully dispersed in cetyl alcohol ($C_{16}H_{34}O$) by heating to just above its melting point (~ 56 °C). Above this temperature cetyl alcohol is highly viscous. On cooling to room temperature the particles were not free to rotate making it ideal for rotational hysteresis experiments. This fixing of particles is particular important for rotational hysteresis, as unfixed particles are known to give rise to spurious effects (Keller, 1997). The relative weakness of the samples collected in oil, meant that they were too weak to be measured on the rotation hysteresis magnetometer.

Throughout this paper the contribution of very small SD grains will be discussed. They are detected by examining the change from a superparamagnetic to stable SD state or *vice versa*, that is, by examining the blocking volume. Each experiment in this paper has its own measuring rate and hence its own blocking volume. By measuring at more than one temperature, it is possible to detect grains which block between two temperatures, and hence detect grains within certain size ranges. For the experiments in this paper, the blocking diameters at various temperatures for iron, magnetite and maghemite are given in Table 2.

A few samples were examined using a Zeiss DSM 960 SEM with EDX (energy-dispersive spectrometer) facilities. The samples were coated with carbon.

3 Results

3.1 ^{57}Fe Mössbauer spectroscopy.

Mössbauer spectra were measured for all eleven samples at room temperature and for DC5, DC6 and SS2 at 88 K. There was found to be little variation between the samples for both the samples collected with and without oil. Each spectrum could successfully be fitted using two central quadrupole doublets and two magnetic hyperfine split sextets. The line intensities of each sextet were constrained to 3:2:1:1:2:3. One representative sample, *i.e.,* DC6, is discussed in detail and is shown in Figure 1. Mössbauer parameters for this sample are listed in Table 3.

295 K spectrum. The central doublet with isomer shift IS = 0.32 mms^{-1} is typical for high spin Fe^{3+} while the other one with IS = 1.20 mms^{-1} is characteristic of Fe^{2+} (Greenwood & Gibb, 1971). It is very likely that the Fe^{2+} and Fe^{3+} ions are in silicates and/or carbonates originating from weathering of walls and buildings. This interpretation is supported by the large quadrupole splitting QS(Fe^{2+}) = 2.33 mms^{-1} which is a typical feature of Fe^{2+} in oxides, while QS(Fe^{3+}) is typically low for such materials (Greenwood & Gibb, 1971). For both components, the line widths (W) are far above those expected for stoichiometric chemical compounds where W ~ 0.25-0.35 mms^{-1}. Hence, each of the experimental doublets is either composed of several sub-doublets or the nearest-neighbour environments of the Fe^{2+} and Fe^{3+} ions are comparatively inhomogeneous due to the presence of metal cations such as Mg^{2+}, Al^{3+} etc. In particular doublet II has an extremely large line width, W = 1.63 mms^{-1}. Most probably this doublet represents a superposition of at least two Fe^{2+} doublets which cannot be resolved. From relative area fractions of both experimental doublets (Table 3) it is clear that the Fe^{3+} component is more common than Fe^{2+}.

Sextet I with a magnetic hyperfine field of B_{hf} ~ 33.1 T is typical for metallic Fe or alloys consisting of Fe with a very low percentage of transition metal ions such as Cr, Ni, V *etc.* (Wertheim *et al.*, 1964; Stearns, 1966; Sauer & Reynik, 1968). The comparatively large line width W ~ 0.41 mms^{-1} cannot be due to pure Fe metal which gives as a rule W ~ 0.25-0.30 mms^{-1}. There are two possible causes for this; the incorporation of other ions such as metal ions or in steel carbon atoms (Bhide, 1973), or alternatively for a pure metallic Fe absorber, line broadening can originate from a small-particle effect as a consequence of the beginning of relaxation. So called relaxation spectra can occur when the relaxation time is $\tau \sim 10^{-8}$ s, characteristic of the ^{57}Fe Mössbauer effect (Greenwood & Gibb, 1971). For flip times $\tau >> 10^{-8}$ s, a normal spectrum is observed while for $\tau << 10^{-8}$ s the sextet collapses to a paramagnetic doublet or singlet, that is, it is superparamagnetic (SP) (Table 2).

Sextet II with B_{hf} = 49.7 T is indicative of γ-Fe_2O_3 (maghemite) (Greenwood & Gibb, 1971; Morris *et al.*, 1985). Our experimental IS = 0.33 mms^{-1} and QS ~ 0 mms^{-1} are consistent with this assignment; in the cited literature for γ-Fe_2O_3 it is reported IS = 0.27-0.41 mms^{-1} and QS ~ 0 mms^{-1}. In general the outermost lines of the sextet of synthetic γ-Fe_2O_3 exhibits W ~ 0.5-0.6 mms^{-1} (Annersten & Hafner, 1973). The measured value of W = 0.84 mms^{-1} in this paper is slightly larger which indicates either a slight deviation from pure maghemite or secondly to a small-particle relaxation effect.

Previous Mössbauer spectroscopy studies have commonly identified other minerals such as hematite (α-Fe_2O_3), magnetite (Fe_3O_4) and goethite (α-FeOOH) (*e.g.*, Hoffmann *et al.*, 1996; Weber *et al.,* 2000; Kopcewicz & Kopcewicz, 1992; 1998; 2001). We could not detect any Fe_3O_4 phase in our samples. Such a component would show two peaks at 295 K in the negative velocity region between v = -7.5 and -8.5 mms^{-1} which we could not observe. No α-FeOOH phase was identified which would exhibit a magnetic hyperfine field of B_{hf}(300 K) = 36 -

38 T (Takada *et al.*, 1964; Forsyth *et al.*, 1968). Similarly no hematite was observed as its B_{hf}(300 K) = 51.5 (Greenwood & Gibb, 1971).

The identification of only maghemite and not magnetite in our samples may seem surprising, but if we consider only studies with very similar collection techniques then magnetite is often not detected, *e.g.*, Mahieu *et al.* (1976) detected maghemite not magnetite, and Tong *et al.* (2001) claimed to have detected only hematite, however, on closer inspection of their data it appears that they have misidentified maghemite for hematite. They did not find magnetite. The exception to this rule are the studies of Kopcewicz & Kopcewicz (1992; 1998; 2001).

88 K spectrum. Both central doublets have slightly increased IS values relative to the 295 K spectrum due to the well known temperature dependence of IS. While no large change in QS(Fe^{3+}) is expected, the temperature-independent QS(Fe^{2+}) demonstrates that the energy difference between the first excited state and the energy ground state of Fe^{2+} is relatively high (Greenwood & Gibb, 1971).

A typical feature of sextet II is the greatly increased intensity of sextet II compared to the 295 K value relative to the other contributions. This increase is partly at the cost of the Fe^{3+} doublet (Table 3). This effect can arise when SP particles are present at 295 K which give rise to the doublet, whilst at 88 K the same particles may have $\tau >> 10^{-8}$ s and they contribute to the sextet associated with γ-Fe_2O_3. There are several potential candidates for this behaviour; SP γ-Fe_2O_3, SP α-FeOOH and SP α-Fe_2O_3. We must first examine the central doublet with QS(295 K) = 0.72 mms^{-1} in closer detail (Figure 1). For SP γ-Fe_2O_3 such a high QS value is interpreted in terms of cation vacancies in the spinel lattice which contribute to a large electric field gradient, which in turn leads to a large QS. The above QS is compatible with a value which can be estimated from a plot in a paper which deals with the temperature dependence of Mössbauer spectra of ultrafine ?-Fe_2O_3 particles (Moskowitz *et al.*, 1997). While at 88 K an α-FeOOH sextet would approximately have the required B_{hf} value, for SP α-FeOOH particles a QS(300 K) = 0.35 mms^{-1} was observed (Rossiter & Hodgson, 1965; van der Kraan & van Loef, 1966), *i.e.*, by far too low for the central Fe^{3+} doublet (Table 3). Another possible candidate is α-Fe_2O_3 , however, B_{hf} (88 K) ~ 54 T is above the required value and at room temperature SP α-Fe_2O_3 as 18 nm particles with QS(300 K) ~ 0.20 mms^{-1} (Kündig *et al.*, 1966) is not compatible with the measured 0.72 mm s^{-1}. After these considerations, it is assumed that primarily cation-ion deficient maghemite gives rise to the Mössbauer spectra temperature effects, *i.e.*, maghemite grains in the grain size range 10-16 nm (Table 2). In contrast Kopcewicz & Kopcewicz (1992; 1998; 2001) identified significant levels of SP α-Fe_2O_3 not SP γ-Fe_2O_3. It is not correct to directly infer from the relative area percentage (Table 3), the relative volume of grains in this grain-size range, however, it can be stated that a significant number of the total number of maghemite grains are in the range 10-16 nm. Another possible cause for the apparent relative increase in maghemite, might be due to oxidation. The 88 K pattern was recorded several months after the 295 K spectrum. For this reason, we suspect that during this time the surfaces of metallic Fe particles (exposed to air) might have been oxidised. Oxidation of Fe particles can also have occurred to

a certain extent during sampling (~ 3 weeks). These oxidation surfaces are possibly maghemite which would contribute to sextet II.

One last unexplained point is the increased line width W = 1.70 mms^{-1} of sextet II relative to W = 0.88 mm/s at 295 K. One possible source which also explains the slightly reduced B_{hf} values is the contribution of relaxation phenomena. For the inner lines of the sextet a detailed analysis could not be made because of the limited spectral resolution.

3.2 Magnetic measurements.

3.2.1 High-temperature susceptibility.

High-temperature susceptibility curves were measured for all the samples collected without oil except DC1 and DC3. A representative curve is shown for DC6 in Figure 2. Generally the curves displayed similar behaviour, that is, on heating there was a very small peak in the curve in the range of 200-300 °C, followed by a wide Hopkinson-like peak near 500 °C, before approaching a Curie point (T_C) in the range 550-590 °C indicating the presence of a magnetite-like phase (T_C = 580 °C, Dunlop & Özdemir, 1997). Calculated Curie temperatures are shown in Table 4. The wide Hopkinson-like peak suggests a wide grain size distribution of small particles of possibly various mineralogies. It was not possible to heat above this temperature, as above 600 °C the sample rapidly altered causing the program to fail. This effect was believed to be due to the rapidly reducing environment which occurs in the CS3 system (Dekkers *et al.*, 2000). At 600 °C the susceptibility did not reduce to zero for samples DC4, DC6 (Figure 2) and SS1, suggesting either the presence of a second magnetic phase with a Curie temperature above this temperature, *e.g.,* hematite (T_C = 675 °C), maghemite (T_C = 645 °C, also inverts to hematite in the range 250-750 °C) or metallic iron (T_C = 765 °C, Dunlop & Özdemir, 1997), or possibly a paramagnetic contribution from the iron ions. On cooling from 600 °C the intensity of the susceptibility was seen to increase, suggesting the formation of a new magnetic phase. The small peak in the range 200-300 °C was greatly enhanced on the cooling. A small reduction in the calculated values for T_C was also observed for the cooling curves (Table 4). To test the alteration effects during heating, a few samples were heated up to only 400 °C. The curves were found to be reversible.

3.2.2 High-temperature thermomagnetic curves.

High-temperature thermomagnetic curves were measured in a field of 100 mT for all the samples collected without oil (Figure 3 and Table 4). The VFTB system was more robust than the CS3 system allowing for heating to 690 °C. The curves display similar behaviour to the high-temperature susceptibility data, with a very weak peak during heating at around 100-200 °C with a second peak at ˜ 500 °C, before dropping sharply in the range 560-600 °C (Figure 3). On heating above 600 °C, the magnetisation was seen to decrease gradually to the maximum available temperature of ˜ 690 °C, indicating the presence of a second magnetic phase. The samples were not held at this temperature to reduce the possibility of oxidation.

The Curie temperatures for the two dominant phases were calculated from the thermomagnetic warming curves. The higher T_C should be treated with caution as there appears to be significant alteration during heating above ˜ 600 °C, as the heating curve is not parabolic. The lower temperature T_C was calculated using a parabolic extrapolation, and the higher T_C using the second-derivative method described in Tauxe (1998). The first T_C was in the range 600-615 °C, whilst the second less well defined T_C, was in the range 638-658 °C (Table 4). The first T_C is indicative of the presence of either maghemite or cation-deficient magnetite, whilst the second T_C is only likely to be that of metallic iron or a second maghemite-like phase (Dunlop & Özdemir, 1997). The second phase is unlikely to be hematite due to its relatively small spontaneous magnetisation making it difficult to observe in the presence of other magnetic minerals such as maghemite. On cooling, the thermomagnetic curves displayed a single magnetic phase with T_C ˜ 580 °C, indicating the presence of magnetite. The magnetite phase would appear to be formed from the two phases during heating (*cf.* Figures 2 and 3).

3.2.3 Low-temperature thermomagnetic curves.

A few low-temperature warming and cooling curves were measured to assess the presence of small SD grains which are SP at room temperature only, stoichiometric multidomain (MD) magnetite and hematite (Nagata *et al.*, 1964). The grain-size ranges with blocking temperatures between 80 K and room temperature are given in Table 2 for magnetite, maghemite and metallic iron. In Figure 4 the warming and cooling curves for two IRMs induced in DC5 in a field of 0.5 T at 80 K and room temperature are shown. There is seen to be a gradual decrease in magnetisation on warming the low-temperature IRM to room temperature, which is due to a combination of the decrease in spontaneous magnetisation, MD re-organisation effects (Muxworthy & McClelland,, 2000) and the unblocking of SP grains. The cooling curve displays only a very slight increase on cooling. In neither case is there evidence for either the Verwey transition or the Morin transition, implying an absence of both MD stoichiometric magnetite and hematite in significant quantities. This supports the Mössbauer spectroscopy data and high-temperature thermomagnetic data. Similar low-temperature behaviour has been observed for fly-ashes (Kapička *et al.*, *2*000).

3.2.4 Low- and room-temperature hysteresis

Magnetic hysteresis measurements were made at room temperature for all the samples, and at 80 K for samples DC5, DC6, SS1, SS2 and SS5 (Figure 5 and Table 5). Generally the hysteresis curves at room temperature were saturated or nearly saturated by 230 mT, with the exception of DC5 (Figure 5) and DC6, therefore all the hysteresis parameters measured using the smaller field given in Table 5 are thought to be correct. The hysteresis loops were narrow and display behaviour for pseudo-single domain (PSD) (Tauxe, 1998). The hysteresis properties for the samples are also summarised in a “Day” plot (Figure 6, Day *et al.*, 1977). It is seen that the samples plot to the right of the region normally associated with PSD grains, which is indicative of the presence of SP grains in combination with other grains types, *i.e.,* SD, PSD and MD, because H_{CR}/H_C ratios are increased by the presence of SP grains (Jackson *et al.*,

*1*990). To truly test whether oil was effective at trapping small particles it would be necessary to compare samples collected simultaneously with and without oil which was not done. None of the curves were noticeably wasp-wasted (Roberts *et al.*, *1*995*;* Tauxe *et al.*, *1*996), suggesting that the relative content of grains near the SP/SD transition was small. Very small SP grains do not contribute to wasp-wasting.

On measuring the hysteresis properties at 80K, the hysteresis curves were still not completely closed even in a field of 950 mT (Figure 5). There was also seen to be a significant increase in H_C for all the samples (Table 5), however, there are corresponding increases in the other magnetic properties, so that the low-temperature hysteresis parameters plot in similar regions of the Day plot (Figure 6). The increase in H_C may have several contributions; primarily, however, in the absence of MD stoichiometric magnetite which is known to display large increases in H_C below the Verwey transition (Muxworthy, 1999), the increase is likely to be due to the blocking of SP grains of either the same or different mineralogy. The coercive force of small grains which are SP at room temperature, but block on cooling, can increase rapidly as the temperature decreases (Banerjee *et al.*, 2000)

3.2.5 Rotational hysteresis

Rotational hysteresis measurements were made for a selection of samples (see Figures 7 and 8, and Table 6). Due to the low magnetic signals of the PM, only samples collected without oil could be measured. Generally the curves were all quite similar and displayed rotational hysteresis loss (W_{RH}) curves typical for SD and PSD particles (*e.g.,* Schmidbauer, 1988). It is useful to quantify the W_{RH} curves using the nomenclature defined in Keller & Schmidbauer (1999); W_{RHp} is the peak rotational hysteresis loss, W_{1600}/W_{RHp} is the ratio of W_{RH} at the maximum field (1600 mT) to W_{RHp}, H_p is the field value for W_{RHp} and $\Delta H_{1/2}$ describes the quantitatively the width of a peak, *i.e.,* it is the full width at half-maximum. These parameters for the samples are summarised in Table 6. Of particular interest is the parameter W_{1600}/W_{RHp}; non-zero W_{1600}/W_{RHp} ratios reflect a high coercive force component within a sample, that is, there is a source of high anisotropy. In SD grains high W_{1600}/W_{RHp} ratios usually indicates the presence of an exchange anisotropy between a ferri- or ferromagnetic phase with an antiferromagnetic phase. This exchange anisotropy does not exist between two ferri- or ferromagnetic phases, *e.g.*, iron and maghemite, or two anti-ferromagnetic phases. The values for W_{1600}/W_{RHp} are relatively low-compared to those reported in the literature (Day *et al.*, 1970; Manson, 1971), suggesting low-exchange anisotropy, the absence of hematite surface oxidation products or alternatively relatively homogeneous particles. That W_{1600}/W_{RHp} does not completely vanish at high fields (Figure 7) has been reported for synthetic PSD particles (*e.g.,* Schmidbauer, 1988). The position of the peak values, H_p, are seen to fall in to two groups; DC2, DC3 and DC6 have values of around 170 mT, whilst DC4 and DC5 which were sampled at the same time from different locations have slightly lower values, respectively 100 mT and 120 mT (Figure 8 and Table 6). DC4 and DC5 also display the highest W_{RHp} values and the narrowest peaks*,* $\Delta H_{1/2}$ (Figures 7 and 8, and Table 6) suggesting narrower grain size

distributions.

3.2.6 Frequency dependency of susceptibility

The frequency dependency of susceptibility (χ_{FD}) measurements were seen to be on average higher for the samples measured in oil than those collected without oil (Table 5). It is suggested that this reflects the higher collection efficiency of the oil based system, though it may also be due to a different source material. The values of χ_{FD} are slightly higher than those measured for PM in other studies (*e.g.,* Shu *et al.*, *2*001) with a peak value for SS5 of 13 %, which may be due to differences in the method of collection. On direct comparison with the hysteresis data, it is seen that generally the samples which display the highest χ_{FD} values also display the lowest H_C values (Table 5), though there are a few exceptions to this observation. The effect of SP grains in reducing H_C has been well documented (*e.g.,* Jackson *et al.*, 1990; Dekkers & Pietersen, 1992).

3.3 Microscopy observations

SEM observations were made on several representative samples. It was found that the PM most likely to contribute to the magnetic signal, *i.e.,* iron-bearing particles, were grains of generally less than 5 μm in diameter. The iron-bearing particles were generally spherical in shape with rough edges, and were found in relatively small concentrations. It was also observed that the iron-bearing particles were separate individual particles and did not appear to be embedded in any larger particles. The SEM had EDX facilities sensitive to iron, but not to oxygen. It was therefore not possible to quantify the valence state of the iron/iron oxide grains. In addition, as the particles were very small it was difficult to make a more detailed EDX study as many of the grains were smaller than the EDX scanning area.

4 Discussion

4.1 Bulk magnetic parameters

There have been several studies of the magnetic properties of atmospheric aerosols or samples thought to be primarily comprise of atmospheric PM, however, as there has been no consistent collection method, it makes direct comparison with other studies difficult.

The high-temperature susceptibility measurements and the thermomagnetic curves, suggest the presence of two magnetic phases; one maghemite-like phase and one iron/maghemite phase. On comparison with the Mössbauer spectroscopy data, it is suggested that the high-temperature phase is iron which altered on heating. Several other studies of urban-particulate or fly-ash have not detected high-temperature phase with a Curie temperature above 600 °C (*e.g.,* Dekkers & Pietersen, 1992*;* Matzka, 1997; Hoffmann *et al.*, *1*999), though high-temperature phases have been observed for house-dust (Matzka, 1997) and by Kapička *et al.*

(2000) for fly-ashes. On carefully reading the characterisation techniques employed in previous magnetic studies, it is seen that many were not sufficient to clearly distinguish between these two iron oxides. Mössbauer spectroscopy is the best method for identifying maghemite in these phases, it is therefore suggested that previous magnetic studies may have mistakenly identified magnetite instead of maghemite.

Only a few studies have examined the magnetic hysteresis properties of atmospheric urban PM (*e.g.,* Matzka, 1997; Muxworthy *et al.*, *2*001), though a few have measured hysteresis curves of fly-ash (*e.g.,* Dekkers & Pietersen, 1992*;* Flanders, 1994; 1999; Kapička *et al.*, *2*000). The H_C values for the samples collected without oil, are generally a little higher than those reported for samples collected by filter methods, and those with oil are little lower (Matzka, 1997; Muxworthy *et al.*, *2*001). This difference is attributed to the increased efficiency of SP grain collection when oil is used. Compared to the fly-ash samples, the hysteresis properties are similar at both room-temperature and liquid nitrogen temperature (Dekkers & Pietersen, 1992). Dekkers & Pietersen (1992) also attributed their measured hysteresis behaviour to the presence of SP grains. The H_{CR} values are close to those reported for urban-PM measured by Hunt *et al.* (1984).

The magnetic phase formed on heating to above 650 °C had magnetite-like characteristics with a Curie temperature of ˜ 580 °C (Figure 3 and Table 4). To further analyse this second phase, hysteresis curves were measured for heated samples at room temperature (Figure 9). It is seen in Figure 9 that the hysteresis curve measured after heating, saturates in a lower field (˜ 150 mT) than the pre-heated hysteresis curve. This lowering of the required saturating field would be expected if metallic iron oxidised to magnetite (Maher *et al.*, 1999).

If the magnetic signal is assumed to be dominated by one mineral, then it is possible to tentatively make grain size estimates from hysteresis parameters, assuming from the SEM observations that the grains are in the PSD range and not dominated by a SD signal. Considering H_C at room temperature ($\mu_0 H_C$ = 4-10 mT) gives rough estimates for the grain size range for metallic iron of 0.2 μm to 0.7 μm (Kneller & Luborsky, 1963) and maghemite of 0.2 μm to 1 μm (Argyle & Dunlop, 1990). It should be noted, that very thin oxidation surfaces are not thought to strongly effect the room temperature magnetic properties of metallic iron (Zhao *et al.*, 1996). The corresponding estimates from the hysteresis curves measured at liquid nitrogen temperature ($\mu_0 H_C$ = 8-14 mT) are approximately 0.15-0.3 μm for metallic iron (Kneller & Luborsky, 1963) and approximately 0.1-0.5 μm for magnetite/maghemite (Dunlop, 1973). If the room-temperature M_{RS}/M_S ratio is considered, this gives rough estimates for metallic iron of ˜ 0.1 μm (Kneller & Luborsky, 1963) and for magnetite/maghemite of also ˜ 0.1 μm (Argyle & Dunlop, 1990). The presence of SP grains will reduce both H_C and M_{RS}/M_S, giving rise to over-estimates of the grain size. These diameters are a little lower on average than those found by Fruhstorfer & Niessner (1994), who analysed grain-size distributions of Munich PM using SEM/EDX analysis. They found that most iron-bearing particles were greater than 1 μm.

From the absolute M_S values (Table 5), it is possible to accurately determine the total magnetic content if only one known mineral phase is present (*e.g.,* Muxworthy *et al.*, 2001), however, when there is more than one phase it becomes more difficult. Here rough estimates are made; considering only metallic iron gives concentration by mass of ~ 0.02-0.4 %, and for only maghemite ~ 0.06-1.2 %. This is in approximate agreement with concentrations reported previously (Department of the Environment, 1996; Muxworthy *et al.,* 2001). An attempt was made to estimate the relative contributions of metallic iron and maghemite by fitting cumulative log Gaussian functions (Stockhausen, 1998) to the DC back field curves from which H_{CR} was derived. It should be realised with this technique that only particles carrying a remanence make a contribution. Associating the higher coercive force component with metallic iron, the results in general gave ~ 30 % metallic iron and ~ 70 % maghemite by remanence. From the thermomagnetic curves (Figure 3) it is also possible to obtain rough estimates for the relative content; ~ 60-70% maghemite and the rest metallic iron.

4.3 Superparamagnetic content

Of great interest to health related studies are the very small grains within PM, as these are the grains most likely to be inhaled into the lungs. In the previous section the bulk or primary magnetic parameters were discussed. In this section evidence for the smallest grain sizes is assessed. These very small grains are normally detected by examining SP behaviour. Previous magnetic PM studies have tried to estimate the magnetic SP content, in particular Xie *et al.* (1999) and Shu *et al.* (2001) have applied the partial-susceptibility technique (von Dobeneck 1998) to determine the different grain size fractions within the samples. In this technique the total SP content is derived from χ_{FD}, and in these two studies, the SP content has been calculated to be as high as 100 %. However, the results must be treated with caution, as this simplified approach seriously underestimates the stable SD content.

In this study, four independent methods which are related to the SP content have been employed; χ_{FD} at room temperature and Mössbauer spectroscopy, and hysteresis and remanence measurements as a function of temperature. Noting that the measuring rate is approximately the same for hysteresis and remanence measurements, then three different measuring rates were employed which effect different regions of the grain size distribution (Table 2).

There is a certain size range of grains which are SP to Mössbauer spectroscopy at room temperature and contribute to the doublet, which block on cooling to 80 K and contribute to the sextet. From Figure 1 maghemite grains in the size range 10-16 nm were identified. No iron in the grain size range 2.5-4 nm was detected (Table 3).

From the χ_{FD} and remanence measurements it is not possible to conclude anything about the mineralogy of the SP grains, only that there are either maghemite or metallic iron grains in the grain-size ranges given in Table 2. On comparison of the low-temperature cooling curve with the warming curve for DC5 (Figure 4), it is possible to roughly estimate the relative SP magnetic content of the sample (Roberts *et al.*, 1995), as the cooling curve is subject only to

the small increase in spontaneous magnetisation, assuming no MD kinematic cooling effects (Muxworthy & McClelland, 2000). It is seen that sample DC5 has nearly 22 % of its magnetic remanence due to grains with blocking temperatures between 80 K and room temperature.

Hysteresis curves can also provide evidence for the presence of SP grains (Roberts *et al.*, 1995; Tauxe *et al.,*1996), especially when measured at low-temperature and at room temperature. To assess the presence of SP grains, it is beneficial to examine both the difference in magnetisation (ΔM) between ascending and descending portions of the hysteresis loop and the derivative of ΔM ($d(\Delta M)/d(B)$) (Tauxe *et al.*, 1996). In Figure 10, ΔM and $d(\Delta M)/d(B)$ are depicted for sample DC5 at both room temperature and liquid nitrogen temperature. DC5 was the sample to show the largest variation in its magnetic properties on cooling to liquid nitrogen temperature (Table 5). On comparison of the two normalised ΔM curves (Figure 10a), it is seen that the effect of cooling is to increase ΔM in the region 100-150 mT. The derivative of $the\ \Delta M$ curves reveals the distribution of coercivities more clearly (Figure 10b). The $d(\Delta M)/d(B)$ curve for the hysteresis curve measured at room temperature, displays a single peak at ˜ 50 mT, suggesting overlapping coercivity spectra for the two magnetic phases. In addition, there is an increase in $d(\Delta M)/d(B)$ on approach to the origin, which is a possible indicator of grains near the blocking volume. The $d(\Delta M)/d(B)$ curve for the hysteresis curve measured at liquid nitrogen temperature displays a second peak at 150 mT, which is associated with the increase in ΔM in the region 100-150 mT. Assuming that this second peak is due to the blocking of room-temperature SP grains of either metallic iron or maghemite, then as the coercive force of metallic iron rises much more sharply on passing through the blocking temperature than maghemite (Kneller & Luborsky, 1963; Dunlop & Özdemir, 1997), it is tentatively suggested that this second peak is due to iron. If this is the case, then this peak must be associated with metallic iron grains between approximately 5 and 8 nm (Table 2).

4.4 Comparison with meteorological data

To understand variations within the data set, the magnetic data was compared to the meteorological data, collected at the Meteorology Institute located in the same building as the Institute for Geophysics. In a previous study (Muxworthy *et al.*, 2001) strong correlations between the relative humidity (RH) and the hysteresis properties of urban PM were found, in particular high RH was found to preferentially remove small particles. For this study, the RH data for Munich was only available for the autumn of 2000. In Figure 11, the RH is plotted as a function of time with χ_{FD} which is a rough indicator of the very smallest grain sizes. Also depicted is H_C. It is seen in this figure that the higher χ_{FD} values loosely correspond to the lowest peaks in the RH in agreement with the conclusions of Muxworthy *et al.* (2001). However, in the present study due the long time sampling it was difficult to draw strong comparisons, between the magnetic and meteorological data due to the large variability in the meteorological data during the collection period, apart from making broad generalisations; samples DC4, DC5, DC6 and SS3 were collected during periods of relatively dry, calm weather, whereas the other samples were collected during peoples of greater variability. It is

seen that the peak deposition rates corresponds with the calmer periods (Table 1).

4.5 Origin of magnetic minerals in PM samples

Generally two magnetic phases appear to be contained within the samples; a maghemite and a metallic iron phase. Firstly it must be considered whether the two phases have separate origins, or whether maghemite is just an oxidation product of iron, that is, a ´two-shell´ particle model with a metallic Fe core and a thin surface oxidation layer. Maghemite, hematite and magnetite have all been reported as surface oxidation products of iron (Zhao *et al.*, 1996; Banerjee *et al.*, 2000). This question is very difficult to resolve, because in terms of bulk magnetic properties any thin surface layer will be magnetically relatively weak. It is known that metallic iron oxidises quickly in air at room temperature, forming a thin oxide surface layer which prevents further oxidation, however, the degree of the thickness of this layer and mineralogy is unknown (Zhao *et al.*, 1996). however, it can be stated from the rotational hysteresis measurements that this surface layer is not hematite. In addition as there was no evidence for magnetite in any of the experiments, it can be indirectly inferred that any surface layer is maghemite. On consideration of the high ratio of maghemite to metallic iron, it is suggested that in this study there were two sets of particles; an independent maghemite phase and an iron phase with a maghemite shell.

The bulk magnetic parameters whether due to maghemite or metallic iron suggest a mean grain size in the region of approximately 0.1-0.7 μm. However, automobiles' exhaust emissions are also known to contribute significantly to the grain-size fraction less than 100 nm (Department of the Environment, 1996), and in particular it has been found that diesel- and petrol engines produce high proportions of nanoparticles (< 10 nm, Shi *et al.*, 2001). That maghemite grains were found in the grain-size range 10-16 nm is consistent with grain-size distribution studies, and there is speculative evidence from the hysteresis data for metallic iron PM in the grain size range 5-8 nm. However, what is of greater interest is the ability to characterise the chemical composition of these ultrafine PM. Only a few studies of ultrafine PM matter have attempted to chemically characterise the PM where iron rich phase have been detected (Hughes *et al.*, 1998), however, these studies do not reveal information about the oxidation state of the iron.

To the authors' knowledge there has been only one previous observation of metallic iron of non-industrial PM, which was from a study of house dust collected in Munich at the Institute of Geophysics (Matzka, 1997). As metallic iron has not been observed in numerous urban PM studies (*e.g.,* Mahieu *et al.*, 1976; Weber *et al.*, 2000), it would therefore appear that this metallic iron phase derives from a non-automobile source. The most likely source for this would be the street-trams which run along Barerstrasse. This assumption was checked by considering dust collected directly from the road surface of a street with no street-trams, following the collection method of Xie *et al.* (1999; 2000). Although this method is not ideal, it provided a rapid collection technique in areas where it was impractical to use the in-house PM

collector. Street dust was collected from Amalienstrasse which runs parallel to Barerstrasse and is approximately 300 m further east. For comparison of this type of sample, a street dust sample was also collected from Barerstrasse, and Mössbauer spectra measured for both samples. It was found that the Barerstrasse sample contained significant levels of metallic iron, whereas no iron was detected in the sample from Amalienstrasse. This finding seems to support the suggestion that the metallic iron loading was derived from street-tram, and the maghemite loading from automobiles. In previous studies iron oxides have been directly associated with automobiles in particular with exhaust emissions (*e.g.,* Hunt *et al.*, 1984, Matzka & Maher, 1999).

5 Conclusion

Urban atmospheric particulate matter collected using a self-designed PM collector, has been studied using a combination of Mössbauer spectroscopy and various magnetic techniques, in an attempt to characterise urban PM collected in central Munich. It has been found that the primary magnetic components are maghemite and metallic iron particles with mean magnetic grain sizes in the range 0.1-0.7 μm.

The detection of maghemite is surprising as previous magnetic studies of urban PM, have reported the detection of magnetite rather than maghemite. Unfortunately due to the different magnetic properties of metallic iron and maghemite it is not possible to give accurate values for their total mass within the sample, however, it was estimated from the magnetic measurements that the concentrations by mass were ~ 0.02-0.4 % for metallic iron, and ~ 0.06-1.2 % for maghemite. The ratio of metallic iron to maghemite by mass was estimated at 1:7. A significant number of maghemite particles in the grain size range 10-16 nm were identified, and there was evidence for metallic iron in the grain size range 5-8 nm. It is believed that the maghemite comes from automobiles, and that the metallic iron comes directly from street-trams which run near to the two sampling locations.

Both iron and iron oxides have been shown to potentially damage the human lung (Donaldson *et al.*, 1998; Phumala *et al.*, 1999; Garçon *et al.,* 2000, Han *et al.*, 2001). However, the evidence suggests that metallic iron is more dangerous than iron oxides due to its higher oxidative stress capabilities (Donaldson *et al.*, 1998). It has been shown that iron induces or acts as a catalyst to produce free radicals such as the hydroxyl radical which is known to cause tissue inflammation which can lead to asthma-like symptoms, pulmonary tumours *etc.* (Phumala *et al.*, 1999; Han *et al.*, 2001). Of particular danger is the presence of nanometre size (< 10 nm) PM, which has been shown to be produce more lung injury than larger particles for the same deposited mass, although the exact mechanism for this effect is uncertain (Donaldson *et al.*, 1998). If our tentative assumption is correct, that nanometre-size metallic iron is produced by street-trams, then this raises questions about the suitability of current designs of street-trams, however, it should be noted that the evidence from this study also suggests that the relative concentration of nanometre-sized metallic iron is small compared to the total grain-size distribution. It must be stressed that more work is needed to examine this

problem.

Acknowledgements

We would like to thank for J. Matzka for our fruitful discussions, and also we thank M. Dekkers and an anonymous reviewer for their comments on the manuscript. We would like to thank L. Sagnotti for use of the CS3 susceptometer at the Istituto Nazionale di Geofisica, Rome. H. Lösslein (Meteorology Institute, University of Munich) kindly provided the meteorological data. Dr. Zettler of F. W. Klever GmbH, helped us with the initial tests on the suitability of using Ballistol oil, for which we are grateful. Finally we would like to thank the workshop at the Institute for Geophysics, University of Munich, for helping in the design and for constructing the PM collectors. This work was funded by the European Union (contract no. ERBFMRXCT-98-0247), as part of the European Network for Mineral Magnetic Studies of Environmental Problems (MAG-NET).

References

Annersten, H. & Hafner, S., 1973. Vacancy distribution in synthetic spinels of the series Fe_3O_4 - γ-Fe_2O_3. *Z. Kristallogr.*, **137**, 321-340.

Argyle, K. S. & Dunlop D. J., 1990. Low-temperature and high-temperature hysteresis of small multidomain magnetites (215-540 nm), *J. Geophys. Res.*, **95**, 7069-7083.

Banerjee, S., Roy, S., Chen, J. W. & Chakravorty, D., 2000. Magnetic properties of oxide-coated iron nanoparticles synthesized by electrodeposition, *J. Magn. Magn. Mater.*, **219**, 45-52.

Bhide, V. G., 1973, *Mössbauer effect and its applications*, Tata McGraw-Hill, New Dehli.

Bozorth, R. M., 1951. *Ferromagnetism*, Van Nostrand, Toronto.

Chantrell, R. W., El-Hilo, M. & O'Grady K., 1991. Spin-glass behavior in a fine particle system, *IEEE Transactions on Magnetics*, **MAG-27**, 3570-3578.

Day, R., O'Reilly, W. & Banerjee, S. K., 1970. Rotational hysteresis study of oxidized basalts, *J. Geophys. Res.*, **75**, 375-386.

Day, R., Fuller, M. & Schmidt, V. A., 1977. Hysteresis properties of titanomagnetites: grain-size and compositional dependence, *Phys. Earth Planet. Inter.*, **13**, 260-266

Dedik, A. N., Hoffmann, P. & Ensling, J., 1992. Chemical characterization of iron in atmospheric aerosols. *Atmos. Environ.,* **26A**, 2545-2548.

Dekkers, M. J. & Pietersen, H. S., 1992. Magnetic properties of low-Ca fly-ash: a rapid tool for Fe-assessment and a survey of potentially hazardous elements, in Advanced Cementitious Systems: Mechanisms and Properties, **245**, pp 37-47, eds. Glasser, F. P., McCarthy, G. J., Young, J. F., Mason, T. O. & Pratt, P. L., Materials Research Society Symposium Proceedings.

Dekkers, M. J., Passier, H. F. & Schoonen, M. A. A., 2000. Magnetic properties of hydrothermally synthesized greigite (Fe_3S_4), II. High- and low-temperature characteristics, *Geophys. J. Int.*, **141**, 809-819.

Department of the Environment, 1996. *Airborne particulate matter in the United Kingdom, Third Report of the Air Quality of Urban Air Review Group*, Department of the Environment, UK.

Donaldson, K., Li, X. Y. & MacNee, W., 1998. Ultrafine (nanometre) particle mediated lung injury, *J. Aerosol Sci.*, **29**, 553-560.

Dunlop, D. J., 1973. Superparamagnetic and single-domain threshold sizes in magnetite, *J. Geophys.*

Res., **78**, 1780-1793.

Dunlop D. J. & Özdemir, Ö., 1997. *Rock magnetism; Fundamentals and Frontiers*, Cambridge University Press, Cambridge.

Flanders, P. J., 1994. Collection, measurement, and analysis of airborne magnetic particulates from pollution in the environment (invited), *J. Appl. Phys.*, **75**, 5931-5936.

Flanders, P. J., 1999. Identifying fly-ash at a distance from fossil fuel power stations, *Environ. Sci. & Tech.*, **33**, 528-532.

Forsyth, J. B., Hedley I. G. & Johnson, C. E. 1968. The magnetic structure and hyperfine field of goethite (α-FeOOH), *J. Phys. C (Proc. Phys. Soc.)*, **1**, 179-188.

Fruhstorfer, P. & Niessner, R., 1994. Identification and classification of airborne soot particles using automated SEM/EDX, *Mikrochim. Acta,* **113**, 239-250.

Garçon, G., Shirali, P., Garry, S., Fontaine, M., Zerimech, F., Martin A. & Hannothiaux, H., 2000. Polycyclic aromatic hydrocarbon coated onto Fe_2O_3 particles: assessment of cellular membrane damage and antioxidant system disruption in human epithelial lung cells (L132) in culture, *Toxic. Lett.*, **117**, 25-35

Gillies, J. A., Gertler, A. W., Sagebiel, J. C. & Dippel, W. A., 2000. On-road particulate matter ($PM_{2.5}$ and PM_{10}) emissions in the Sepulveda Tunnel, Los Angeles, California, *Environ. Sci. & Techn.*, **35**, 1054-1063.

Greenwood, N. N. & Gibb, T. C., 1971. *Mössbauer spectroscopy*. Chapman and Hall Ltd., London.

Han, J-Y, Takeshita, K. & Utsumi, H., 2000. Non-invasive detection of hydroxyl radical generation in lung by diesel exhaust particles, *Free Rad. Bio. Med.*, **30**, 516-525.

Harrison, R. M. & Yin, J., 2000. Particulate matter in the atmosphere: which particle properties are important for its effects on health? *Sci. Total Environ.,* **249**, 85-101.

Hoffmann, P., Dedik, A. N., Ensling, J., Weinbruch, S., Weber, S., Sinner, T., Gütlich, P. & Ortner, H. M., 1996. Specification of iron in atmospheric aerosol samples, *J. Aerosol Sci.,* **27**, 325-337.

Hoffmann, V., Knab, M. & Appel, E., 1999. Magnetic susceptibility mapping of roadside pollution, *J. Geochem. Exp.*, **66**, 313 B 326.

Hughes, L. S., Cass, G. R., Gone, J., Ames, M. & Olmez, I., 1998. Physical and chemical characterization of atmospheric ultrafine particles in the Los Angeles area, *Environ. Sci. & Tech.*, **32**, 1153-1161.

Hunt, A., Jones, J. & Oldfield, F., 1984. Magnetic measurements and heavy metals in atmospheric particulates of anthropogenic origin, Sci. Total Environ., 33, 129-139.

Jacobs, L. S. & Luborsky, F. E., 1957. Magnetic anisotropy and rotational hysteresis in elongated fine-particle magnets, J. Appl. Phys., 28, 467-473.

Jackson, M. J., Worm, H.-U., Banerjee, S. K., 1990. Fourier analysis of digital hysteresis data: rock magnetic applications, *Phys. Earth Planet. Inter.*, **65**, 78-87.

Jacobs, L. S. & Luborsky, F. E., 1957. Magnetic anisotropy and rotational hysteresis in elongated fine-particle magnets, J. Appl. Phys., 28, 467-473.

Kapička, A., Jordanova, N., Petrovský, E. & Ustjak, S. 2000. Magnetic stability of power-plant fly-ash in different soil solutions, *Phys. Chem. Earth.*, **25**, 431-436.

Keller, R., 1997. Magnetische Eigenschaften und Rotationhysterese von Titanomagnetitpartikeln $Fe_{3-x}Ti_xO_4$ der Zusammensetzung x = 0.6 und x= 0.7 in der Größe von Einbereichs-, Pseudoeinbereichs- und Vielbereichsteilchen, *Ph.D. Thesis,* University of Munich.

Keller, R. & Schmidbauer, E., 1999. Magnetic hysteresis properties and rotational hysteresis losses of synthetic stress-controlled titanomagnetite ($Fe_{2.4}Ti_{0.6}O_4$) particles-II. Rotational hysteresis losses, *Geophys. J. Inter.*, **138**, 334-342.

Kim, W-S., Kim, S. H., Lee, D. A., Lee, S., Lim, C. S. & Ryu, J. H., 2000. Size analysis of automobile

soot particles using field-flow fractionation, *Environ. Sci. & Tech.*, **35**, 1005-1012.

Kneller, E. F. & Luborsky, F. E., 1963. Particle size dependence of coercivity and remanence of single-domain particles, *J. Appl. Phys.*, **34**, 656-658.

Kopcewicz, B. & Kopcewicz, M., 1992. Seasonal variations of iron concentration in atmospheric aerosols. *Hyperfine Inter.*, **71**, 1457-1460.

Kopcewicz, B. & Kopcewicz, M., 1998. Iron-containing atmospheric aerosols. *Hyperfine Inter.*, **111**, 179-187.

Kopcewicz, B.; Kopcewicz, M., 2001. Long-term measurements of iron-containing aerosols by Mössbauer spectroscopy in Poland, *Atmos. Environ.*, **35**, 3739-3747.

Kündig, W., Bömmel, H., Constabaris, G. & Lindquist, R. H., 1966. Some properties of supported small α-Fe_2O_3 particles determined with the Mössbauer effect, *Phys. Rev.,* **142**, 327-333.

Maher, B. A., Thompson, R. & Hounslow, M. W., 1999. Introduction, in *Quaternary Climates, Environments and Magnetism*, pp. 1-48, eds. Maher, B. A., & Thompson, R., Cambridge Univ. Press, Cambridge.

Mahieu, B., Ladriere, J. & Desaedeleer, G., 1976. Mössbauer spectroscopy of airborne particulate matter, *J. Phys. Coll.*, C6, **12**, C6-837-C6-840.

Manson, A. J., 1971. Rotational hysteresis measurements on oxidized synthetic and natural titano-magnetites, *Z. Geophys.*, **37**, 431-442.

Matzka, J., 1997. Magnetische, elektronenmikroskopische und lichtmikroskopische Untersuchungen an Stäuben und Aschen sowie an einzelnen Aschepartikeln, *Diplomthesis*, University of Munich.

Matzka, J. & Maher, B. A., 1999. Magnetic biomonitoring of roadside tree leaves: identification of spatial and temporal variations in vehicle-derived particles, *Atmos. Environ.*, **33**, 4565-4569.

Meiklejohn, W. H. & Bean, C. P., 1957. New magnetic anisotropy. *Phys. Rev.*, **105**, 904-913.

Morris, R. V., Lauer, H. V., Lawson, C. A., Gibson, E. K., Nace, G. A. & Stewart, C., 1985. Spectral and other properties of submicron powders of hematite (α-Fe_2O_3), maghemite (γ-Fe_2O_3), magnetite (Fe_3O_4), goethite (α-FeOOH), and lepidocrocite (γ-FeOOH). *J. Geophys. Res.,* **90**, 3126-3144.

Morris, W. A., Versteeg, J. K., Bryant, D. W., Legzdins, A. E., McCarry, B. E. & Marvin, C. H., 1995. Preliminary comparisons between mutagenicity and magnetic susceptibility of respirable airborne particulate, *Atmos. Environ.*, **29**, 3441-3450.

Moskowitz, B. M., Frankel, R. B., Walton, S. A, Dickson, D. P. E, Wong, K. K. W., Douglas T. & Mann S., 1997. Determination of the pre-exponential frequency factor for superparamagnetic maghemite particles in magnetoferritin, *J. Geophys. Res.*, **102**, 22671-22680.

Muxworthy, A. R., 1999. Low-temperature susceptibility and hysteresis of magnetite. *Earth Planet. Sci. Lett.*, **169**, 51-58.

Muxworthy, A. R., 2002. Magnetic hysteresis and rotational hysteresis properties of hydrothermally grown multidomain magnetite, *Geophys. J. Inter.*, **in press.**

Muxworthy, A. R. & McClelland, E., 2000. The causes of low-temperature demagnetization of remanence in multidomain magnetite, *Geophys. J. Inter.*, **140**, 132-146.

Muxworthy, A. R., Matzka, J. & Petersen, N., 2001. Comparison of magnetic parameters of urban atmospheric particulate matter with pollution and meteorological data, *Atmos. Environ.*, **35(26)**, 4379-4386.

Nagata, T., Kobayashi, K. & Fuller, M. D., 1964. Identification of magnetite and hematite in rocks by magnetic observations at low temperature, *J. Geophys. Res.*, **69**, 2111-2120.

Olson, K. W. & Skogerboe, R. K., 1975. Identification of soil lead compounds from automotive sources. *Environ. Sci. & Tech.*, **9**, 227-230.

Phumala, N., Ide, T. & Utsumi, H., 1999. Non-invasive evaluation of *in vivo* free radical reactions catalysed by iron using *in vivo* ESR spectroscopy, *Free Rad. Bio. Med.*, **26**, 1209-1217.

Roberts, A. P., Cui Y-L. & Verosub, K. L., 1995. Wasp-waisted hysteresis loops: mineral magnetic characteristics and discrimination of components in mixed magnetic systems, *J. Geophys. Res.*, **100**, 17909-17924.

Rossiter M. J. & Hodgson A. E. M., 1965. A Mössbauer study of ferric oxy-hydroxide, *J. Inorg. Nucl. Chem.*, **27**, 63-71.

Sauer, W. E. & Reynik, R. J., 1968. Solid-solution strengthening in Fe-Cr alloys using Mössbauer spectroscopy, in *Mössbauer Effect Methodology*, **4**, pp. 201- 225, ed. Gruverman, I. J., Plenum Press, New York.

Schmidbauer, E., 1988. Magnetic rotational hysteresis study on spherical 85-160 nm Fe_3O_4 particles, *Geophys. Res. Lett.*, **15**, 522-525.

Shi, J. P, Evans, D. E., Khan, A. A. & Harrison, R. M., 2001. Sources and concentration of nanoparticles (< 10 nm diameter) in the urban environment, *Atmos. Environ.*, **35**, 1193-1202.

Shu, J., Dearing, J. A., Morse, A. P., Yu, L. & Li, C., 2001. Magnetic properties of daily sampled total suspended particulates in Shanghai, *Environ. Sci. &Tech.*, **34**, 2393-2400.

Stacey, F. D. & Banerjee, S. K., 1974. *The Physical Principles of Rock Magnetism*, Elsevier, Amsterdam.

Stearns, M. B., 1966. Spin-density oscillations in ferromagnetic alloys. I. “localized” solute atoms: Al, Si, Mn, V, and Cr, in Fe. *Phys. Rev.*, **147**, 43-453.

Stockhausen, H., 1998. Some new aspects for the modelling of isothermal remanent magnetisation acquisition curves by cumulative log Gaussian functions. *Geophys. Res. Lett.,* **25**, 2217-2220.

Takada, T., Kiyama, M., Bando, Y., Nakamura, T., Shiga, M., Shinjo, T., Yamamoto, N., Endoh, Y. & Takaki, H., 1964. Mössbauer study of α-, β-, and γ- FeOOH. *J. Phys. Soc. Japan,* **19**, 1744-1750.

Tauxe, L., 1998. *Paleomagnetic principles and practice*, Kluwer Academic Publishers, Dordrecht.

Tauxe, L., Pick, T. & Mullender, T. A. T.., 1996. Wasp-waists, pot-bellies, and superparamagnetism, *J. Geophys. Res.*, **101**, 571-583.

Tong, Y., Li, A., Cai, Y., Ni, X., Zhang, Y., Wang, J., Guo, P., Li, X. & Zhang, G., 2000. Mössbauer study of atmospheric aerosols of Shanghai, *Environ. Sci. & Tech.,* **35**, 1342-13476.

van der Kraan, A. M. & van Loef, J. J., 1966. Superparamagnetism in submicroscopic α-FeOOH particles observed by the Mφssbauer effect, *Phys. Lett.,* **20**, 614-616.

von Dobeneck, T., 1998. The concept of partial susceptibilities, *Geol. Carpath.*, **49**, 228-229.

Veranth, J. M., Smith, K. R., Huggins, F., Hu, A. A., Lighty, J. S. & Aust, A. E. 2000. Mössbauer spectroscopy indicates that iron in an aluminosilicate glass phase is the source of the bioavailable iron from coal fly ash, *Chem. Res. Toxicol.,* **13**, 161-164.

Weber, S., Hoffmann, P., Ensling, J., Dedik, A. N., Weinbruch, S., Miehe, G., Gütlich, P. & Ortner, H. M., 2000. Characterization of iron compounds from urban and rural aerosol sources, *J. Aerosol Sci.,* **31**, 987-997.

Wertheim, G. K., Jaccarino, V., Wernick, J. H. & Buchanan, D. N. E., 1964. Range of exchange interaction in iron alloys, *Phys. Rev. Lett.*, **12**, 24-27.

Xie, S., Dearing, J. A. & Bloemendal, J., 1999. A partial susceptibility approach to analysing the magnetic properties of environmental materials: a case study, *Geophys. J. Int.*, **138**, 851-856.

Xie, S., Dearing, J. A. & Bloemendal, J., 2000. The organic content of street dust in Liverpool, UK, and its association with dust magnetic properties, *Atmos. Environ.*, **34**, 269-275.

Zhao, X. Q.; Liu, B. X.; Liang, Y. & Hu, Z. Q., 1996. Oxidation behavior and magnetic properties of metallic ultrafine particles, *J. Magn. Magn. Mater.,* **164**, 401-410.

Table 1. Details of sampling dates and techniques, and the daily mass collected for each sample in the study. The dust collectors were cleaned on the first day of the sampling period,

and the PM collected on the last as described in the text. Location 1 was approximately 15 m from Barerstrasse whilst location 2 was approximately 80 m from the same street. Two models of dust collecter were used (M1 and M2) as discussed in the text. For M1 the number in brackets refers to the diameter of the PM collector and the number of collectors used. For dust collector M2 it was possible to cover the base of the collector with a thin layer of oil. The oil was thought to help prevent particles from being removed by wind during the sampling period. The mass was not obtained when the samples were collected in oil.

Sample	Dates	Location	Model	oil	mass (mgm^{-2} per day)
DC1	5/10/99-19/9/99	2	M1 (2 m)	no	5.1
DC2	19/9/99-5/10/99	1	M1 (2 m)	no	13
DC3	24/9/99-8/10/99	1	M1 (1.4 m)	no	6.3
DC4	8/10/99-19/10/99	2	M1 (2 x 1.4 m)	no	14
DC5	8/10/99-21/10/99	1	M1 (2 m + 1.4 m)	no	26
DC6	21/10/99-16/11/99	1	M1 (2 m + 1.4 m)	no	22
SS1	24/8/00-11/9/00	2	M2	no	13
SS2	12/9/00-4/9/00	2	M2	yes	…
SS3	4/10/00-2/11/00	2	M2	yes	…
SS4	2/11/00-6/12/00	2	M2	yes	…
SS5	6/12/00-27/12/00	2	M2	yes	…

Table 2. Blocking diameters for Mössbauer spectroscopy (sampling rate of 10^{-8} s), remanence measurements (10 s), and χ_{FD} for the frequencies described in the text. It is assumed that the hysteresis and remanence measurements have the same sampling frequency. The blocking diameter for magnetite at room temperature and for metallic iron at liquid nitrogen are an experimental observations, whilst the maghemite blocking diameter at room temperature for the remanence measurements is based on experimental observations of magnetite. The other values in the table are calculated from these experimental values using the standard blocking volume equation (Dunlop & Özdemir, 1997). The blocking diameters are in nanometres. The estimate for the blocking diameter of maghemite at room temperature is higher than that observed for non-stoichiometric maghemite 20-27 nm (Moskowitz *et al.*, 1997), but lower than the theoretical estimate of 42 nm by Chantrell *et al.* (1990). It is seen that the effect of cooling covers a much wider range of grain sizes than just measuring χ_{FD} at room temperature.

mineral	Mössbauer		Hysteresis & remanence		χ_{FD} range
	90 K	300 K	80 K	300 K	
metallic iron	2.5	4	5.1*	8.4	6.4-6.8
magnetite	9	14	18	30¶	23-25
maghemite	10	16	22	35†	28-30

* Kneller & Luborsky (1963)
¶ Dunlop (1973)
† calculated from experimental measurements on magnetite.

Table 3. Fitted Mössbauer parameters for spectra of Figure1 (sample DC6) . IS = isomer shift (with reference to metallic iron); QS= quadrupole splitting; B_{hf} = magnetic hyperfine field; W = line width (full width of the peak at half the maximum peak value (FWHM)) (for sextets W refers to the outermost lines as is the convention); rel. area (%) = relative area fraction of a doublet or a sextet with respect to the area of the whole fitted spectrum.

		IS (mms^{-1})	QS (mms^{-1})	Bhf(T)	W(mms^{-1})	rel. area (%)
doublet I	295 K	0.32	0.74	…	0.57	55.6
	88 K	0.45	0.77	…	0.62	44.7
Doublet II	295 K	1.2	2.3	…	1.63	23.9
	88 K	1.22	2.86	…	0.56	13
sextet I	295 K	~ 0	-0.02	33.2	0.41	10.9
	88 K	0.09	-0.03	33.9	0.44	10.8
sextet II	295 K	0.33	-0.09	49.7	0.84	9.6
	88 K	0.46	-0.14	49.8	1.7	31.5

Table 4. Curie temperatures for the high-temperature thermomagnetic and susceptibility heating and cooling curves, calculated using the second derivative method as described in Tauxe (1998), except for the lower Curie temperatures of the thermomagnetic heating curves. These was determined using a parabolic extrapolation. The field applied during the thermomagnetic measurements was 100 mT. The maximum temperature for the susceptibility measurements was 600 °C, and for the thermomagnetic curves it was 690 °C.

sample	High-temperature χ		Thermomagnetic analysis		
	Heating	cooling	Heating		cooling
	T_C (°C)	T_C (°C)	T_C (°C)	T_C (°C)	T_C (°C)
DC2	552	555	600	652	578
DC3	…	…	615	653	578
DC4	586	569	610	658	584
DC5	589	…	615	658	578
DC6	582	576	600	638	577
SS1	577	573	600	…	…

Table 5. Summary of magnetic hysteresis data at both room temperature and liquid nitrogen temperature, plus the frequency dependency of magnetic susceptibility measured at room temperature. Field corresponds to the maximum field applied during hysteresis.

Sample	temp.	field	$\mu_0 H_C$	$\mu_0 H_{CR}$	M_{RS}	M_S	M_{RS}/M_S	χ_{FD}
	(K)	(mT)	(mT)	(mT)	(mAm^2kg^{-1})	(mAm^2kg^{-1})		(%)
DC1	293	230	8.4	39	6	52	0.12	9
DC2	293	230	9.1	44	26	180	0.14	4
DC3	293	230	8.9	42	31	220	0.14	†
DC4	293	230	8.9	39	54	400	0.14	†
DC5	293	950	10	50	81	810	0.1	2
	80	950	14	60	110	880	0.13	…
DC6	293	950	7.8	48	70	820	0.09	2
	80	950	11	53	110	890	0.12	…
SS1	293	230	7	30	55	400	0.13	7
SS2	293	950	5.2	33	¶	¶	0.06	4
	80	950	8.4	45	¶	¶	0.09	…
SS3	293	950	6.3	40	¶	¶	0.08	8
	80	950	11	55	¶	¶	0.1	…
SS4	293	230	7.6	35	¶	¶	0.12	12
SS5	293	950	7.8	38	¶	¶	0.09	13
	80	950	12	54	¶	¶	0.1	…

¶ sample collected in oil, and the mass was not measured.

† samples too weak to measure.

Table 6. Rotational hysteresis parameters defined in Keller & Schmidbauer (1999); where W_{RHp} is the peak rotational hysteresis loss, W_{1600}/W_{RHp} is ratio of W_{RH} at the maximum field (1600 mT) to W_{RHp}, H_p is the field value for W_{RHp} and $\Delta H_{1/2}$ describes the quantitatively the width of a peak, *i.e.,* it is the FWHM. A high W_{1600}/W_{RHp} ratio is an indicator of an extremely high anisotropy, *e.g.*, an exchange anisotropy, H_p is loosely related to H_C and $\Delta H_{1/2}$ is represents the width of the coercive force spectra.

sample	W_{RHp} (mJkg^{-1})	W_{1600}/W_{RHp}	H_p (mT)	$\Delta H_{1/2}$ (mT)
DC2	3.3	0.3	170	350
DC3	5.4	0.1	170	300
DC4	6.4	0.16	100	290
DC5	10.6	0.094	116	290
DC6	7.5	0.13	170	300

Figure 1. Mössbauer spectra measured for DC6 at both room temperature and 88 K.

Figure 2. High-temperature susceptibility curve measured for sample DC6. Heating was in air.

Figure 3. High-temperature thermomagnetic curve measured for DC2. The applied field was 100 mT, and the heating was conducted in air. A paramagnetic correction has been made.

Figure 4. Low-temperature isothermal remanence (IRM) heating and cooling curves for DC5. The IRMs were induced in a field of 0.5 T.

Figure 5. Detail of hysteresis curves for DC5 measured at 300 K and 80 K. The maximum applied field was 0.95 T. The inset shows the entire spectra.

Figure 6. M_{RS}/M_S versus H_{CR}/H_C (Day plot) for all the hysteresis data shown in Table 5. The ratios are classified in terms of the measuring temperature and whether the sample had been collected using oil or not (see Table 1).

Figure 7. Rotational hysteresis loss versus field for sample DC4.

Figure 8. Detail of rotational hysteresis loss for samples DC2-6.

Figure 9. Hysteresis curves measured for DC6 before heating and after heating to 690 °C in air. The maximum applied field was 230 mT. The absolute values of the saturation magnetisation increased by 25 % after heating for DC6, which is similar to that of DC2 (Figure 3).

Figure 10. (a) shows the change of magnetisation M as function of field (ΔM). The curve has been smoothed. (b) the derivative of ΔM ($d(\Delta M)/d(B)$) as a function of field, for sample DC5. The “wiggles” at approximately 400 mT are due to noise.

Figure 11. Relative humidity (line), χ_{FD} (●) and H_C (○) as a function of time for samples SS1-SS5. Note SS1 was measured with no oil, whereas the other samples were measured with oil. The sampling period was September to December, 2000.

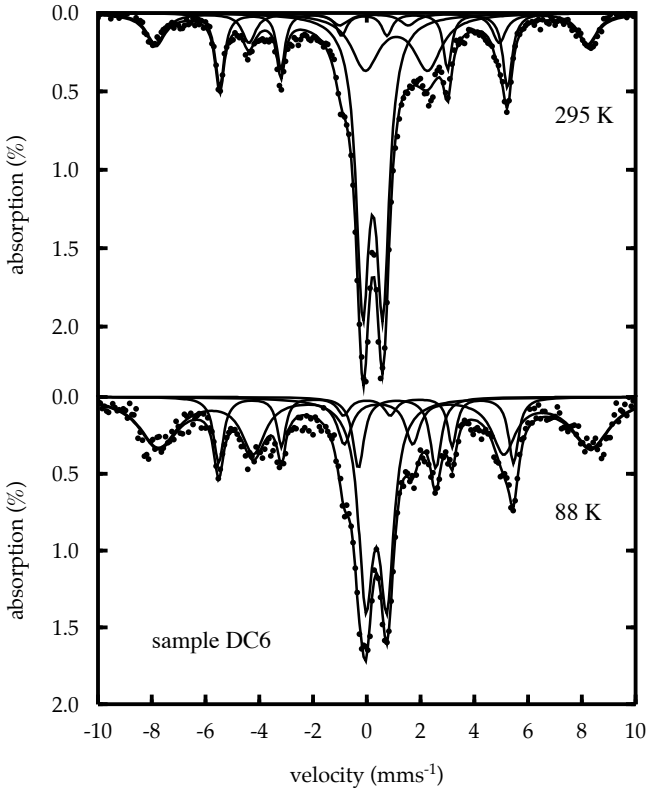
0.0
0.5
1.0
1.5
2.0
absorption (%)
295 K
0.0
0.5
1.0
1.5
2.0
absorption (%)
88 K
sample DC6
-10
-8
-6
-4
-2
0
2
4
6
8
10
velocity (mms-1)

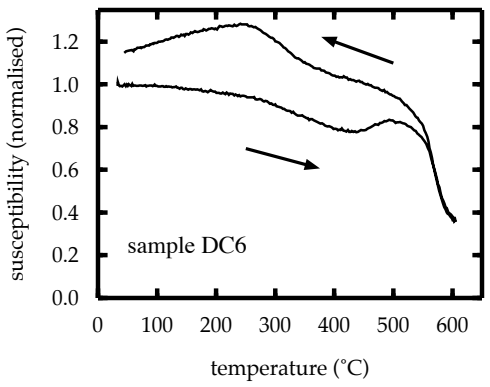
susceptibility (normalised)
1.2
1.0
0.8
0.6
0.4
0.2
0.0
sample DC6
0
100
200
300
400
500
600
temperature (˚C)

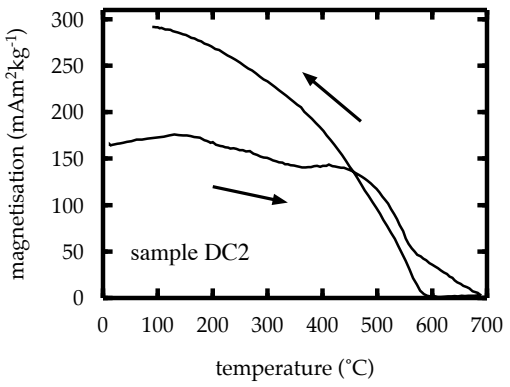
magnetisation (mAm^{2}kg^{-1})
300
250
200
150
100
50
0
sample DC2
0
100
200
300
400
500
600
700
temperature (°C)

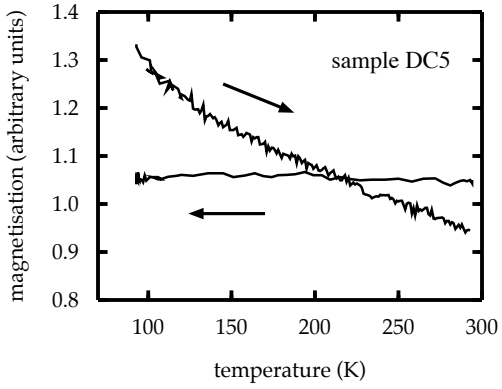
sample DC5
magnetisation (arbitrary units)
temperature (K)
1.4
1.3
1.2
1.1
1.0
0.9
0.8
100
150
200
250
300

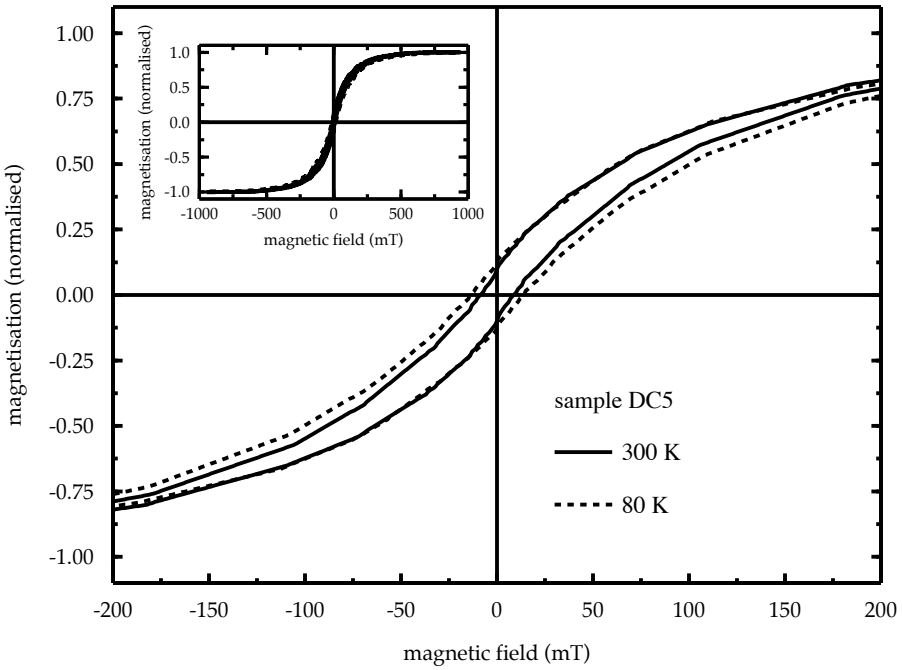
magnetisation (normalised)
magnetic field (mT)
sample DC5
300 K
80 K
magnetisation (normalised)
magnetic field (mT)

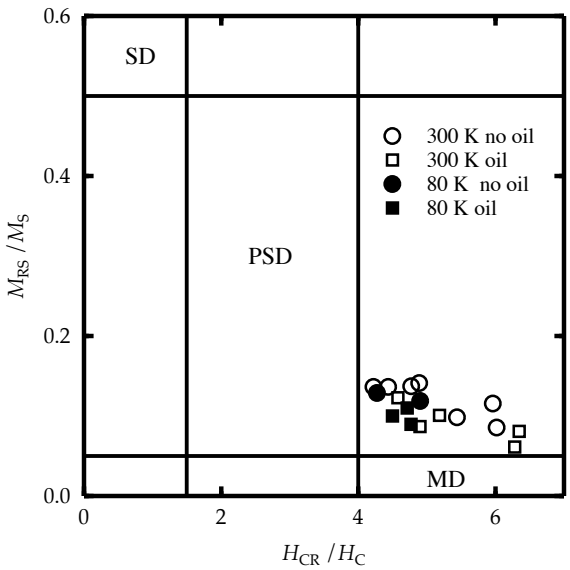
0.6
0.4
0.2
0.0
0
2
4
6
SD
PSD
MD
300 K no oil
300 K oil
80 K no oil
80 K oil
M_{RS}/M_S
H_{CR}/H_C

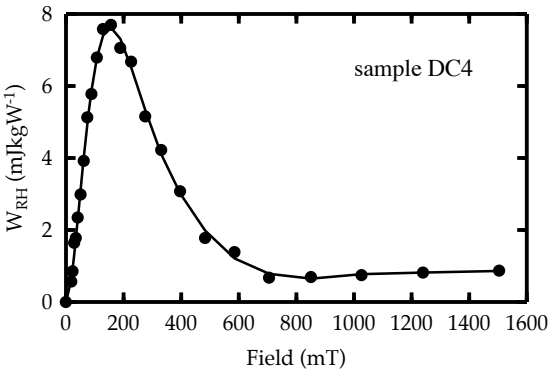
sample DC4
W_{RH} (mJkgW^{-1})
Field (mT)
0
2
4
6
8
0
200
400
600
800
1000
1200
1400
1600

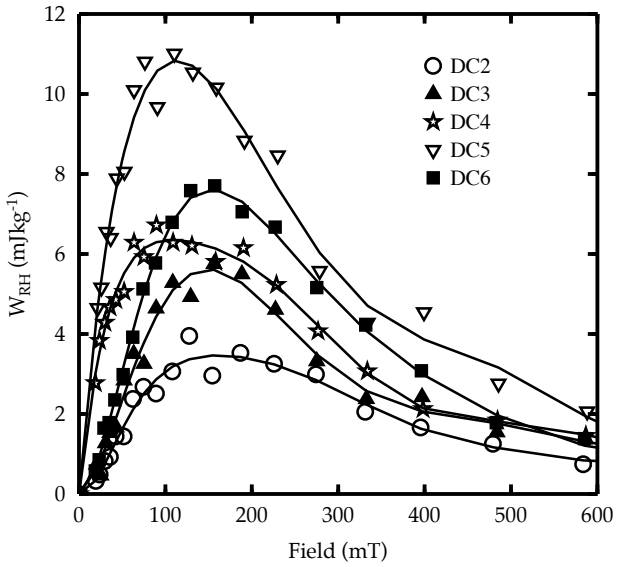
12
10
8
6
4
2
0
0
100
200
300
400
500
600
Field (mT)
W_{RH} (mJkg^{-1})
DC2
DC3
DC4
DC5
DC6

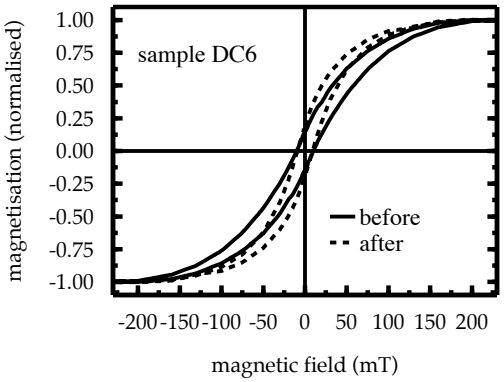
sample DC6
before
after
magnetisation (normalised)
1.00
0.75
0.50
0.25
0.00
-0.25
-0.50
-0.75
-1.00
-200 -150 -100 -50 0 50 100 150 200
magnetic field (mT)

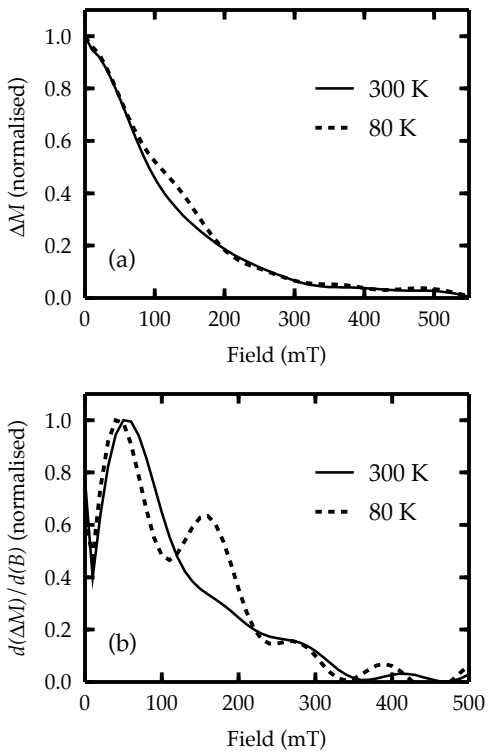
1.0
0.8
0.6
0.4
0.2
0.0
ΔM (normalised)
300 K
80 K
(a)
0
100
200
300
400
500
Field (mT)
1.0
0.8
0.6
0.4
0.2
0.0
d(ΔM) / d(B) (normalised)
300 K
80 K
(b)
0
100
200
300
400
500
Field (mT)

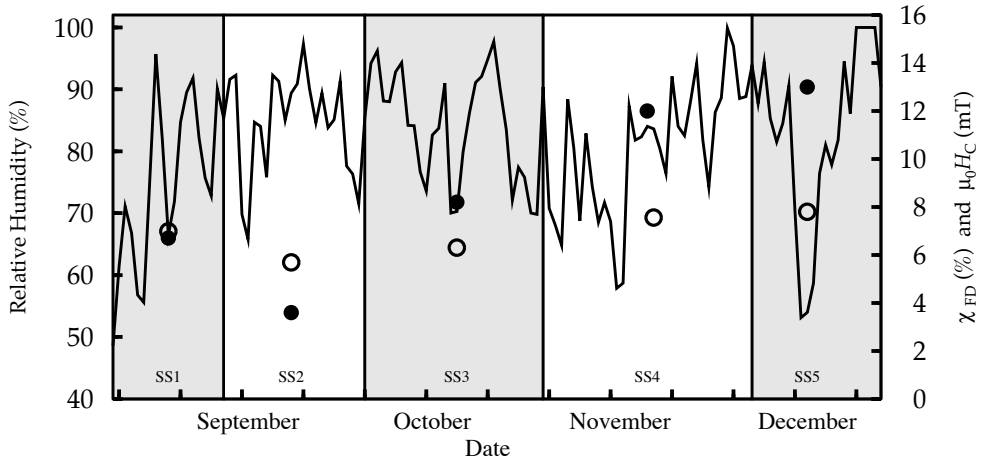
Relative Humidity (%)
100
90
80
70
60
50
40
16
14
12
10
8
6
4
2
0
χ FD (%) and μ0HC (mT)
SS1
SS2
SS3
SS4
SS5
September
October
November
December
Date